RSC Advances

PAPER

Check for updates

Synthesis, structural and magnetic properties of cobalt(II) complexes with pyridine-based macrocyclic ligand containing two pyridine pendant arms†

Eva Zahradníková, [ID] [a] Céline Pichon, [ID] [b] Carine Duhayon,[b] Jean-Pascal Sutter, [ID] *[b] Petr Halaš[a] and Bohuslav Drahoš [ID] *[a]

With the aim of tuning the magnetic anisotropy, a series of Co(II) complexes with the general formula of complex cations $[Co(L)X]^+$, where X = Br^- (**1**); I^- (**2**); NCO^- (**3**); NCS^- (**4a**); N_3^- (**5**), and $[Co(L)(NCS)_2]$ (**4b**), (L = a 17-membered pyridine-based N_3O_2-macrocyclic ligand containing two pyridin-2-ylmethyl pendant arms) were prepared and thoroughly characterized. The molecular structures for all complexes showed strongly distorted geometry in between octahedral and trigonal prismatic. The magnetic studies confirmed substantial magnetic anisotropy with positive values of D, the axial zero-field splitting parameter, but E/D ratios close to 1/3. This was supported by theoretical CASSCF calculations showing no significant effect of the co-ligands. Complex **4b** was found to behave as a field-induced SMM.

Introduction

Magnetoactive complexes, especially single-molecule magnets (SMMs), represent an interesting family of compounds, where a slow relaxation of the magnetization of purely molecular origin occurs below a blocking temperature.[1,2] SMMs do not rely on magnetic ordering unlike "classical" magnets, thus they are potential materials for ultra-dense information storage, quantum computing, molecular switches, or spintronics.[3–5] SMMs are characterized by an energy barrier, U, between two states corresponding to the opposite direction of the magnetic moment. This barrier depends both on the spin of the system S, and on the value of the axial zero-field splitting parameter D. The original efforts to increase the value of U were based on increasing the number of total spin, however, this turned out to be at the expense of the overall magnetic anisotropy.[6,7] On the other hand, tuning the magnetic anisotropy of individual magnetic centers by appropriate ligand design and modulation of the coordination sphere has been more successful.[8,9] Macrocyclic ligands appear particularly interesting because they can induce less frequent coordination numbers or maintain

specific/required coordination geometry of the central atom, and lead to interesting magnetic behaviors.[10–12]

Co(II) complexes represent the second most studied group of SMMs[13] after Dy(III) complexes.[14,15] Various structures based mainly on acyclic ligands (Schiff bases, heterocycles, polypyridines) have been intensively investigated,[16] whereas those with macrocyclic ligands are rather scarce. Furthermore, the coordination sphere, *i.e.* the geometry and strength of the ligand field, has a crucial effect on magnetic anisotropy and consequently on the relaxation of magnetization as well,[17–19] which is valid not only for Co(II) compounds, but also for all other complexes including Dy(III)-based SMMs.

The synthesis of 15-membered pyridine-based macrocyclic ligand **15-pyN₃O₂** (see Fig. 1) was described more than 30 years ago,[20] and complexes with 3d transition metals have been studied mainly in the field of molecular magnetism and medicine. The first study concerned Mn(II) complexes as potential MRI contrast agents.[21] Furthermore, a series of complexes with M = Mn, Fe, Co, Ni, Cu, and Zn was prepared. As the radius of the central atom decreased, a decrease in coordination number was observed from 7 for Mn(II), Fe(III), Co(II), through 5 + 2 for Ni(II), 4 + 1 for Cu(II) to 5 for Zn(II). In the case of the Co(II) and Ni(II) complexes, a large axial ZFS component with $D(Co) \approx 40\ cm^{-1}$, $D(Ni) = -6.0\ cm^{-1}$, was found.[11]

Since the Co(II) complex showed an intriguing magnetic behavior, a series of $[Co(\mathbf{15\text{-}pyN_3O_2})X_2]$, where X = Cl^-, Br^-, I^-, was subsequently prepared and studied.[22] All three complexes had coordination number 7 and the shape of the coordination polyhedron corresponded to distorted pentagonal bipyramid and exhibited the behaviour of field-induced SMMs. For this

[a]Department of Inorganic Chemistry, Faculty of Science, Palacký University Olomouc, 17. listopadu 12, CZ-771 46 Olomouc, Czech Republic. E-mail: bohuslav.drahos@upol.cz; Tel: +420 585 634 954; +420 585 634 429

[b]Laboratoire de Chimie de Coordination du CNRS (LCC-CNRS), Université de Toulouse, CNRS, Toulouse, France. E-mail: jean-pascal.sutter@lcc-toulouse.fr
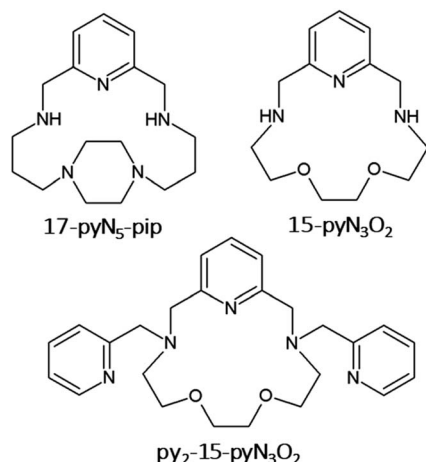
Fig. 1 Structural formulas of the 15- and 17-membered macrocyclic ligands discussed in the text.

geometry of the coordination polyhedron, Co(II) is anticipated to possess a positive D parameter, which was subsequently confirmed in all cases with $D(Cl) = 38$ cm^{-1}; $D(Br) = 41$ cm^{-1}; $D(I) = 35$ cm^{-1}.[22] The correlation between the values of D parameter and the Mayer bond order (decreasing in order Co–I > Co–Cl > Co–Br) was understood as a consequence of the ligand field splitting and the decreasing covalency of the Co–X bond. Whether associated to a Cl, Br, or I anion, all complexes behaved as field-induced SMMs.[22]

Moreover, several derivatives of **15-pyN$_3$O$_2$** decorated with two pendant arms with different functional groups (*e.g.* pyridine,[10] carboxylate,[23] benzimidazol)[24] were prepared. Among them the pyridine derivative **py$_2$-15-pyN$_3$O$_2$** (Fig. 1) was the most interesting as a decrease in coordination number from 7 (Mn^{II}, Fe^{II}, Co^{II}), to 6 + 1 (Ni^{II}), to 5 (Cu^{II}) was observed.[10] For the 7-coordinated complexes, all donor atoms of the macrocyclic ligand were coordinated to the central metal atom and the geometry of the coordination sphere was close to pentagonal bipyramid. In case of Ni(II) complex, the length of Ni–O$_{aliph}$ bond was prolonged to 2.653(3) Å, and for the Cu(II) complex, one pyridine pendant arm and one oxygen atom were not coordinated. Substantial magnetic anisotropy was evidenced for Fe(II), Co(II) and Ni(II) complexes, with $D(Fe) = -7.4(2)$ cm^{-1}, $D(Co) = +34(1)$ cm^{-1}, and $D(Ni) = -12.8(1)$ cm^{-1}.[10] Despite its positive D parameter, the Co(II) complex exhibited slow relaxation of magnetization below 8 K.[10]

On the other hand, for a series of Co(II) complexes with 17-membered pyridine/piperazine-based macrocycle **17-pyN$_5$-pip** (Fig. 1), [Co(**17-pyN$_5$-pip**)X]$^+$ (where X = Cl$^-$, Br$^-$, N$_3^-$, NCO$^-$, NCS$^-$, NCSe$^-$) with distorted trigonal prismatic geometry, a negative D parameter was found with values ranging from -20 to -41 cm^{-1}, and all showed field-induced SMM behavior.[25]

Thus, motivated by the above-mentioned studies, we synthesized a structurally new macrocyclic ligand **py$_2$-17-pyN$_3$O$_2$ = L** (Fig. 2) as a structural analogue of **py$_2$-15-pyN$_3$O$_2$** with an enlarged macrocyclic cavity and its Co(II) complexes with different monovalent halido-/pseudohalido coligands. We investigated the effect of enlarged 17-membered macrocyclic cavity on the molecular structure and coordination geometry of Co(II) centers and compare the coordination ability of this ligand **L** with its 15-membered analogue. Moreover, the effect of coligand exchange on the structural properties as well as on the magnetic behavior of all Co(II) complexes were examined.

Experimental

Materials and methods

All the solvents (VWR International, Fontenay-sous-Blois, France) and other chemicals were purchased from commercial sources (Acros Organics, Geel, Belgium and Sigma-Aldrich, St. Louis, MO, USA) and used as received. Silica gel for column chromatography was purchased from Penta, Prague, Czech Republic (Silica gel 100; 0.063–0.2 mm). A one channel just infusion™ linear pump NE 300 (New Era Pump Systems, Inc., Farmingdale, NY, USA) and HSW Norm-Ject 20 mL syringes were employed during the ligand synthesis (infusion rate 1 mL min^{-1}). ^{1}H and ^{13}C NMR spectra were measured at laboratory temperature on 400 MHz NMR spectrometer Varian MR-400 for high-resolution solution-state NMR (Varian, Palo Alto, CA, USA): ^{1}H 399.95 MHz, (CDCl$_3$, tetramethylsilane) $\delta = 0.00$ ppm, ^{13}C 100.60 MHz, (CDCl$_3$, residual solvent peak) $\delta = 77.0$ ppm. Multiplicity of the signals was indicated as follows: s – singlet, d – doublet, t – triplet, quin – quintet, m – multiplet, br – broad. Deuterated solvent CDCl$_3$, containing 0.03% of TMS, from Sigma-Aldrich was used as received. The atom numbering scheme used for NMR data interpretation is shown in Fig. 2. The carbon as well as hydrogen atoms were assigned according to the spectra obtained from two-dimensional correlation experiments ^{1}H–^{1}H *gs*-COSY, ^{1}H–^{13}C *gs*-HMQC and ^{1}H–^{13}C *gs*-HMBC (see ESI Fig. S1–S5†). The mass spectra were collected on
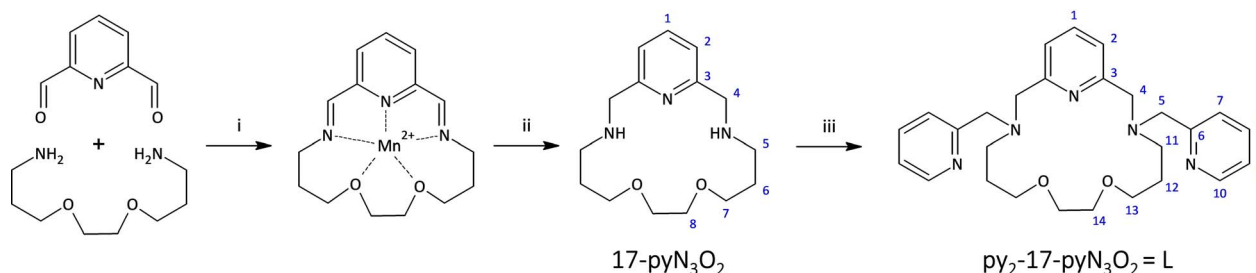

Fig. 2 Synthetic scheme for macrocycles **17-pyN$_3$O$_2$** and **L** together with the atom numbering used for NMR assignment for both macrocycles; (i) MnCl$_2$·4H$_2$O, methanol; (ii) NaBH$_4$, O$_2$, H$_2$O; 73%; (iii) 2-(chlormethyl)pyridine, anhydrous K$_2$CO$_3$, anhydrous acetonitrile; 68%.

an LCQ Fleet mass spectrometer (Thermo Scientific, Waltham, MA, USA) equipped with an electrospray ion source and three-dimensional (3D) ion-trap detector in the positive mode (see ESI Fig. S6–S10†). IR spectra were measured on Jasco FT/IR-4700 spectrometer (Jasco, Easton, MD, USA) using the ATR technique on a diamond plate in the spectral range 4000–400 cm^{-1} (see ESI Fig. S11†). Elemental analysis (C, H, N) was realized on a Flash 2000 CHNO–S analyzer (Thermo Scientific, Waltham, MA, USA).

Magnetic measurements for all the samples were carried out with a Quantum Design MPMS 5S SQUID magnetometer in the temperature range 2–300 K. The measurements were performed on polycrystalline samples mixed with grease and put in gelatin capsules. The temperature dependences of the magnetic susceptibility was obtained in an applied field of 1 kOe and the isothermal field dependence of the magnetizations were collected up to 5 T at temperatures between 2 and 8 K. The molar susceptibility (χ_M) was corrected for sample holder, grease and for the diamagnetic contribution of all the atoms by using Pascal's tables.[26] AC susceptibility data were collected in the frequency range 1–1500 Hz. Assessment of the ZFS parameters have been done considering an $S = 3/2$ spin for Co(II), the software PHI[27] was used for fitting the $\chi_M T = f(T)$ and $M = f(H)$ behaviors. The powder X-ray diffraction (PXRD) patterns were measured on Rigaku Miniflex600 diffractometer in reflection mode with $\lambda(CuK_{\alpha 1}, K_{\alpha 2}) = 1.54059$ and 1.54439 Å radiations (see ESI Fig. S12†).

Crystal data refinement

Single crystals of **1–5** suitable for X-ray structure analysis were prepared as described in the section Synthesis. X-ray diffraction data were collected on XtaLAB (Synergy-i or Synergy-s) Rigaku diffractometers (CuK$_\alpha$ radiation source, $\lambda = 1.54184$ Å) at 293(2) K or at 100 K. The molecular structures of studied complexes were solved by direct methods or SHELXT and refined by full-matrix least-squares based on F^2 (SHELXL 2014/07).[28] Program Olex2 1.3 and CRYSTALS_15.4.2 [29] were used for the final refinement.[30] The hydrogen atoms on carbon atoms were fixed into idealized positions (riding model) and assigned temperature factors either $H_{iso}(H) = 1.2$ Ueq. (pivot atom) for CH and CH$_2$ moieties or $H_{iso}(H) = 1.5$ Ueq. (pivot atom) for CH$_3$ groups. The molecular and crystal structures of the studied complexes, depicted in Fig. 3 and S13–S23† were drawn using the Mercury software.[31] Solvent mask procedure had to be applied to treat the co-crystallized

disordered solvent molecules (one CH$_3$OH molecule for complexes **1, 2, 3, 5** and 0.25 CH$_3$OH molecule for complexes **4a**). Other positional disorders were found in obtained molecular structures – complex **3**: perchlorate anion (occupancy factors 0.39 and 0.61), complex **4a**: uncoordinated NCS- anion (occupancy factors 0.48 and 0.52) and O2–C12–C13 part of the macrocycle (occupancy factors 0.23 and 0.77), complex **5**: perchlorate anion (occupancy factors 0.20 and 0.80) and C11–O2–C12 part of the macrocycle (occupancy factors 0.27 and 0.73).

Synthesis of ligands

Synthesis of parent macrocycle 17-pyN$_3$O$_2$. 7,10-Dioxa-3,14,20-triazabicyclo[14.3.1]icosa-1(20),16,18-triene (**17-pyN$_3$O$_2$**). The macrocycle **17-pyN$_3$O$_2$** was prepared according to the modified literature procedure.[32] Yield: 0.58 g; 73%. ^{1}H NMR (400 MHz, CDCl$_3$): δ 7.45 (t, 1H, H1, $^3J_{HH}$ = 7.8 Hz); 6.96 (d, 2H, H2, $^3J_{HH}$ = 7.8 Hz); 3.79 (s, 4H, H4); 3.48 (m, 8H, H7+8); 2.67 (t, 4H, H5, $^3J_{HH}$ = 6.1 Hz); 2.46 (br.s., –NH–); 1.72 (quin, 4H, H6, $^3J_{HH}$ = 6.1 Hz). ^{13}C NMR (100 MHz, CDCl3): δ 159.22 (C3); 136.43 (C1); 120.63 (C2); 70.79 (C8); 70.63 (C7); 55.32 (C4); 47.52 (C5); 29.89 (C6). MS m/z (+): 280.15 (calcd. 280.20) [**17-pyN$_3$O$_2$**+H]$^+$; 302.14 (calcd. 302.18) [**17-pyN$_3$O$_2$**+Na]$^+$.

Synthesis of the macrocyclic ligand L. 3,14-Bis(pyridin-2-ylmethyl)-7,10-dioxa-3,14,20-triaza-bicyclo[14.3.1]icosa-1(20),16,18-triene (**L**). **17-pyN$_3$O$_2$** (0.72 g; 2.58 mmol) was dissolved in anhydrous acetonitrile (50 mL) and solid anhydrous K$_2$CO$_3$ (3.57 g; 25.8 mmol) was added. 2-(Chloromethyl)pyridine (0.66 g; 5.17 mmol) was dissolved in anhydrous acetonitrile (20 mL) and slowly added during vigorous stirring to the previous mixture. Resulting mixture was refluxed for 3 h. Solid K$_2$CO$_3$ was filtered off on a S4 glass frit, the solvent was evaporated under reduced pressure. Crude product was dissolved in 4 M aqueous solution of NaOH and extracted with chloroform (3 × 15 mL). Organic phases were collected, dried with anhydrous Na$_2$SO$_4$, filtered off with a S4 glass frit and evaporated under reduced pressure. Crude product was then purified by column chromatography on silica gel with gradient elution. As a mobile phase a mixture of ethanol/NH$_4$OH (25% aq.) was used in ratios: 10/1 → 7/1 → 5/1 (75 mL for each ratio). Fractions containing the product were collected. After the solvents were evaporated under reduced pressure, the pure product was obtained as a beige solid. Yield: 0.81 g; 68%. ^{1}H NMR (400 MHz, CDCl$_3$): δ 8.34 (d, 2H, H10, $^3J_{HH}$ = 5.2 Hz); 7.54 (m, 4H, H7 + 8); 7.44 (t, 1H, H1, $^3J_{HH}$ = 7.8 Hz); 7.24 (d, 2H, H2, $^3J_{HH}$ = 7.8 Hz); 6.99 (t,
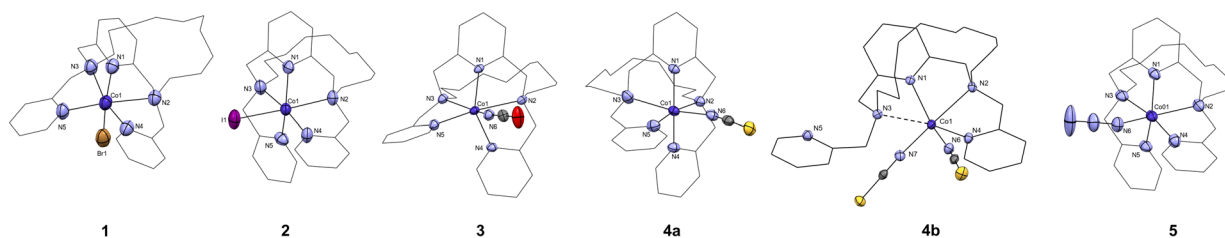

Fig. 3 The molecular structures of the [CoL(X)]$^+$ cations found in the crystal structure of complex **1** (X = Br$^-$), **2** (X = I$^-$), **3** (X = NCO$^-$), **4a** (X = NCS$^-$), **5** (X = N$_3^-$), and the molecular structure of [Co(L)(NCS)$_2$], complex **4b**. Atoms of the coordination sphere are drawn as thermal ellipsoids at the 50% probability level. Hydrogen atoms and anions were omitted, and macrocyclic ligand is drawn as a wireframe for clarity.

Paper

2H, H9, $^3J_{HH}$ = 5.2 Hz); 3.96 (s, 4H, H5); 3.75 (s, 4H, H4); 3.19 (t, 4H, H13, $^3J_{HH}$ = 5.6 Hz); 3.11 (s, 4H, H14); 2.62 (t, 4H, H11, $^3J_{HH}$ = 5.6 Hz); 1.62 (m, 4H, H12). ^{13}C NMR (100 MHz, CDCl$_3$): δ 157.42 (C6); 156.37 (C3); 148.85 (C10); 136.92 (C1); 136.75 (C8); 123.92 (C7); 123.01 (C2); 122.42 (C9); 69.78 (C14); 68.40 (C13); 59.88 (C5); 59.64 (C4); 50.27 (C11); 26.46 (C12). MS m/z (+): 462.20 (calcd. 462.29) [**L** + H]$^+$; 484.21 (calcd. 484.27) [**L** + Na]$^+$.

Complexes preparation and characterization

Caution! Perchlorate salts of complexes are hazardous, heating or scratching them in solid form can lead to an explosion.

Co(II) complexes **1** and **4a** were prepared in the same way. Equimolar amounts of metal salt (71 mg of CoBr$_2$·6H$_2$O or 45 mg of Co(SCN)$_2$·2H$_2$O) and ligand **L** (100 mg; 0.217 mmol) were mixed in methanol (3 mL). The complexes were crystallized by vapor diffusion of diethyl ether into the resulting methanolic solution at 7 °C and the single crystals suitable for X-ray analysis were separated by decantation after three weeks. **4b** was obtained from **4a** after leaving the crystallisation mixture at RT for several days.

Co(II) complexes **2**, **3** and **5** were prepared similarly. Co(ClO$_4$)$_2$·6H$_2$O (79 mg; 0.217 mmol) was dissolved in methanol (2 mL) and tetrabutylammonium iodide (200 mg; 0.541 mmol), NaNCO (70 mg; 1.08 mmol) or NaN$_3$ (56 mg; 1.08 mmol) were added. The solution was filtered and the filtrate was added dropwise to methanolic solution (2 mL) of **L** (100 mg; 0.217 mmol). The complexes were crystallized as mentioned above.

[CoLBr]Br·CH$_3$OH (**1**·CH$_3$OH): Dark green crystals, yield 100 mg (68%). MS m/z(+): 484.31 (calcd. 484.27) [CoL + Na]$^+$; 599.20 (calcd. 599.13) [CoL + Br]$^+$; C$_{28}$H$_{39}$Br$_2$CoN$_5$O$_3$; M_r = 712.38, found (calcd.): C 46.87 (47.21); H 5.45 (5.52); N 9.68 (9.83); IR (ATR, cm^{-1}): 1606, 1579, 1442 [ν(C=C)$_{py}$ + ν(C=N)$_{py}$].

[CoLI]I$_{0.5}$(ClO$_4$)$_{0.5}$·CH$_3$OH (**2**·CH$_3$OH): Dark violet crystals, yield 72 mg (44%). MS m/z(+): 484.32 (calcd. 484.27) [CoL + Na]$^+$; 619.17 (calcd. 619.16) [CoL + ClO$_4$]$^+$; 647.11 (calcd. 647.12) [CoL + I]$^+$; C$_{28}$H$_{39}$Cl$_{0.5}$CoN$_5$O$_5$I$_{1.5}$; M_r = 792.66, found (calcd.): C 42.68 (42.43); H 4.84 (4.96); N 8.66 (8.84); IR (ATR, cm^{-1}): 1605, 1578, 1444 [ν(C=C)$_{py}$ + ν(C=N)$_{py}$]; 1091, 622 [ν(ClO$_4$)$^-$].

[CoL(NCO)]ClO$_4$·CH$_3$OH (**3**·CH$_3$OH): dark violet crystals, yield 92 mg (61%). MS m/z(+): 519.19 (calcd. 519.20) [CoL − H]$^+$; 562.20 (calcd. 562.21) [CoL + NCO]$^+$; C$_{29}$H$_{39}$ClCoN$_6$O$_8$; M_r = 694.04, found (calcd.): C 51.03 (50.19); H 5.59 (5.66); N 12.14 (12.11); IR (ATR, cm^{-1}): 2205 [ν(NCO)$^-$]; 1605, 1583, 1444 [ν(C=C)$_{py}$ + ν(C=N)$_{py}$]; 1077, 621 [ν(ClO$_4$)$^-$].

[CoL(NCS)]NCS·0.25CH$_3$OH (**4a**·0.25CH$_3$OH): violet crystals, yield 60 mg (43%). MS m/z(+): 484.32 (calcd. 484.27) [CoL + Na]$^+$; 578.19 (calcd. 578.19) [CoL + NCS]$^+$; C$_{29.25}$H$_{36}$CoN$_7$O$_{2.25}$S$_2$; M_r = 644.71, found (calcd.): C 53.61 (53.49); H 5.67 (5.63); N 15.01 (15.21); IR (ATR, cm^{-1}): 2050 [ν(N=C=S)$^-$] 1605, 1570, 1467 [ν(C=C)$_{py}$ + ν(C=N)$_{py}$].

[CoLN$_3$]ClO$_4$·CH$_3$OH (**5**·CH$_3$OH): dark blue crystals, yield 53 mg (35%). MS m/z(+): 484.32 (calcd. 484.27) [CoL + Na]$^+$; 562.17 (calcd. 562.22) [CoL + N$_3$]$^+$; C$_{28}$H$_{39}$ClCoN$_8$O$_7$; M_r = 694.04, found (calcd.): C 47.96 (48.46); H 5.38 (5.66); N 16.58 (16.15); IR (ATR, cm^{-1}): 2068 [ν(N$_3$)$^-$]; 1605, 1580, 1444 [ν(C=C)$_{py}$ + ν(C=N)$_{py}$]; 1076, 621 [ν(ClO$_4$)$^-$].

Computation details

ORCA 5.0.4 software package[33] was utilized for all computations. First, complex cations were extracted from crystal structures and positions of hydrogen atoms were optimized using DFT with BP86 functional[34] and def2-TZVP basis set for all atoms except for carbon and hydrogen where less demanding def2-SVP basis set was chosen[35] together with resolution of identity (RI) approximation[36] and def2/J auxiliary basis set.[37] For complex **2**, DKH2 was turned on together with relativistically recontracted DKH2-def2-SVP and TZVP basis sets similarly as before except for iodine where SARC-DKH-TZVP basis set[38] was chosen together with SARC/J auxiliary basis set for Coulomb fitting. Subsequent CASSCF(7,5)/NEVPT2 calculations were performed utilizing the same basis sets as for the optimization calculations with the addition of RIJCOSX approximation[39] and def2-TZVP/C basis set[40] for correlation calculation.

Results and discussion

Synthesis and general characterization of the ligand L

Ligand **L** represents a structurally new compound, and it is a two-carbon longer analogue to the previously prepared ligand **py$_2$-15-pyN$_3$O$_2$** (Fig. 1). The synthesis of the parent macrocycle proceeded analogously to the previously described 17-membered pyridine/piperazine-based ligand **17-pyN$_5$-pip**.[32] For the cyclization step a linear pump was used, which ensures continuous addition of reactants, leading to a significant increase in the reaction yield. In this case 73% yield was achieved. In addition, an optimization of the cyclization reaction was performed on this system and the results are the subject of a forthcoming publication. The next step was a simple substitution reaction with pre-neutralized 2-(chloromethyl)pyridine. After purification of the crude product by column chromatography, the desired product was obtained and subsequently used for the preparation of complexes with selected Co(II) salts.

Synthesis and general characterization of complexes 1–5

Complexes **1** and **4a** were prepared by mixing the Co(II) salt with the ligand in methanol. Complex **4a** transformed to **4b**. The synthesis of complexes **2**, **3** and **5** was divided in two steps: methanolic solution of Co(II) perchlorate was mixed with tetrabutylammonium iodide, NaNCO or NaN$_3$ respectively, then the resulting solution was filtered and the filtrate was then mixed with the methanolic solution of ligand. After diffusion of diethyl ether was finished, highly crystalline solids were obtained for all complexes. The formation of all complexes was subsequently confirmed by mass spectrometry, infrared spectroscopy, elemental analysis and single crystal X-ray analysis. No inert conditions were required as all compounds are air-stable.

IR spectra of all complexes were very similar (see ESI, Fig. S11†). Vibrations corresponding to the macrocyclic ligand can be observed in the positions ∼1600, ∼1580 and ∼1460 cm^{-1} (C=C and C=N aromatic vibrations). For complexes **3–5**, stretching vibrations of the coordinated anions 2068 cm^{-1} (N=N=N), 2205 cm^{-1}, (N=C=O), ∼2050 cm^{-1} (N=C=S) or

perchlorate anion ~1080 and ~620 cm^{-1} were observed as well. Signals in mass spectra (positive mode) always very well corresponded to the [Co(L)X]$^+$ cation, where X = Br$^-$ (**1**); I$^-$ (**2**); NCO$^-$ (**3**); NCS$^-$ (**4a**); and N$_3^-$ (**5**). In case of complexes containing perchlorate counter anions, signal of [Co(**L**)(ClO$_4$)]$^+$ cations was observed as well.

The phase purity of the samples was confirmed by the measurement of X-ray powder diffraction patterns which are comparable to those calculated from cif files for each complex (see ESI Fig. S12†).

X-ray diffraction analysis

All complexes crystallized in the space groups $P2_1/c$ except for, complexes **4a** and **4b** which crystallized respectively in the space groups $P\bar{1}$ and $Pna2_1$. Other crystal data and structure refinements for studied complexes **1–5** are listed in Table 1. The molecular structures of complexes **1–5** are depicted in Fig. 3, S13 and S14.† For **1–3**, **4a**, and **5** the macrocyclic ligand is coordinated to the central Co(II) cation by three nitrogen donor atoms of the macrocyclic cavity and two nitrogen donor atoms belonging to the methylpyridine pendant arms and the last sixth coordination position is occupied by an anionic halido/pseudohalido coligand (Fig. 3). The distances for coordination bonds of all complexes **1–5** are listed in Table 2, selected bond angles are listed in Table S1.† There is no bond between the central metal atom and the two oxygen atoms in the aliphatic

part of the macrocycle (interatomic distance ~5.7 Å). The shortest bonds within the coordination sphere are between Co(II) and the N-donor coligand (NCO, N$_3$) in the range of 2.015–2.044 Å. The length of the bonds to the macrocyclic pyridine ring N1 ranges between 2.059–2.068 Å, followed by slightly longer bonds to the nitrogen atoms N4 and N5 in the pendant arms (2.090–2.210 Å). In contrast, the bonds between the central atom and the aliphatic nitrogen atoms are significantly extended (2.330–2.438 Å), and the longest distance is between the central atom and the halogen anions (2.563 and 2.822 Å for **1** and **2**, respectively).

Complex **4a** underwent a rather scarce crystal-to-crystal transformation to a structurally different new compound **4b**, which was evidenced by measured PXRD patterns (Fig. S12†). The coordination sphere of **4b** (Fig. 3 and S23†) is strikingly different from that of **4a**. Two thiocyanate anions coordinate the central Co(II) atom and only one pyridine pendant-arm is linked to the metal center whereas the second pyridine pendant-arm is uncoordinated. Moreover, the Co–N3 (macrocycle) distance is significantly elongated to ~2.7 Å, suggesting semi-coordination of N3 and final coordination number 5 + 1.

In order to elucidate the nature of Co1–N3 interaction, we performed QT-AIM[41] analysis in the vicinity of these atoms utilizing MultiWFN 3.7 software,[42] as our co-workers utilized this method in previous work.[43] Negative sign(λ_2)ρ value (Fig. S15†) in this region suggests that the interaction should be

Table 1 Crystal data and structure refinements for studied complexes **1–5**

Compound	**1**·MeOH	**2**·MeOH	**3**·MeOH	**4a**·0.25MeOH	**4b**	**5**·MeOH
Formula	C$_{28}$H$_{39}$Br$_2$CoN$_5$O$_3$	C$_{28}$H$_{39}$Cl$_{0.5}$CoI$_{1.5}$N$_5$O$_5$	C$_{29}$H$_{39}$ClCoN$_6$O$_8$	C$_{29.25}$H$_{36}$CoN$_7$O$_{2.25}$S$_2$	C$_{29}$H$_{35}$CoN$_7$O$_2$S$_2$	C$_{28}$H$_{39}$ClCoN$_8$O$_7$
M_r	712.38	792.66	694.04	644.71	636.71	694.04
Temperature (K)	293(2)	293(2)	100.0(1)	100.0(1)	100.0(1)	100.0(1)
Wavelength (Å)	1.54184	1.54184	1.54184	1.54184	1.54184	1.54184
Crystal system	Monoclinic	Monoclinic	Monoclinic	Triclinic	Orthorhombic	Monoclinic
Space group	$P2_1/c$	$P2_1/c$	$P2_1/c$	$P\bar{1}$	$Pna2_1$	$P2_1/c$
a (Å)	9.5063(2)	9.8084(2)	10.1831(3)	9.4553(3)	9.20980(10)	10.2781(4)
b (Å)	16.1542(6)	16.5786(3)	15.8178(4)	9.5655(3)	32.9484(3)	15.7954(4)
c (Å)	19.9926(7)	20.3177(3)	19.9190(6)	18.0521(5)	9.78030(10)	19.6987(5)
α (°)	90	90	90	84.509(2)	90	90
β (°)	95.610(3)	92.489(2)	93.777(3)	85.684(2)	90	95.297(3)
γ (°)	90	90	90	69.475(3)	90	90
V, Å^3	3055.49(17)	3300.73(10)	3201.46(17)	1520.53(8)	2967.81(5)	3184.36(17)
Z	4	4	4	2	4	4
D_{calc}, g cm^{-3}	1.479	1.530	1.373	1.391	1.425	1.381
μ, mm^{-1}	7.714	15.686	5.416	6.023	6.171	5.439
$F(000)$	1380	1516	1380	666	1332	1380
θ range for data collection (°)	3.524–67.684	3.442–67.684	3.571–67.684	4.927–67.684	2.682–73.823	3.593–57.684
Refl. Collected	33 103	17 924	15 118	14 621	30 483	16 491
Independent refl.	5591	5979	5926	5523	6088	5884
$R(int)^a$	0.0524	0.0422	0.0507	0.0403	0.0340	0.0417
Data/restrains/parameters	4030/0/334	5013/0/380	4687/60/434	4906/36/402	5642/1/371	4143/78/462
Completeness to θ (%)	98.8	98.3	98.2	99.0	99.2	97.7
Goodness-of-fit on F^2	1.037	1.032	1.106	1.030	0.953	1.033
R_1, wR_2 ($I > 2\sigma(I)^b$)	0.0538/0.1440	0.0473/0.1282	0.0567/0.1562	0.0624/0.1597	0.0268/0.0730	0.0639/0.1708
R_1, wR_2 (all data)^b	0.0754/0.1591	0.0561/0.1340	0.0710/0.1641	0.0697/0.1647	0.0274/0.0733	0.0881/0.1869
Largest diff. peak and hole/ A^{-3}	1.215/−0.667	0.724/-0.638	0.791/-0.524	1.465/-0.484	0.180/-0.250	0.901/-0.766
CCDC number	2344172	2344178	2344177	2344175	2371458	2344176

^{a} $R_{int} = \sum|F_o{}^2 - F_{o,mean}{}^2|/\sum F_o{}^2$. ^{b} $R_1 = \sum(|\cdot|F_o| - |F_c|\cdot|)/\sum|F_o|$; w$R_2 = [\sum wR_2(F_o - F_o{}^2)^2/\sum w(F_o{}^2)^2]^{1/2}$.

Table 2 Selected bond lengths (Å) for the studied complexes **1–5** together with the calculated structural parameter τ_6

1		2		3		4	4a	4b	5	
Co1–N1	2.059(4)	Co1–N1	2.064(4)	Co1–N1	2.068(3)	Co1–N1	2.059(3)	2.069(1)	Co1–N1	2.065(3)
Co1–N2	2.439(4)	Co1–N2	2.339(4)	Co1–N2	2.433(3)	Co1–N2	2.361(2)	2.280(2)	Co1–N2	2.344(3)
Co1–N3	2.364(4)	Co1–N3	2.409(4)	Co1–N3	2.350(3)	Co1–N3	2.338(4)	2.703(2)	Co1–N3	2.400(4)
Co1–N4	2.099(3)	Co1–N4	2.209(4)	Co1–N4	2.108(3)	Co1–N4	2.090(3)	2.162(2)	Co1–N4	2.159(4)
Co1–N5	2.196(4)	Co1–N5	2.106(3)	Co1–N5	2.166(3)	Co1–N5	2.204(3)	5.455(2)	Co1–N5	2.103(3)
Co1–Br1	2.5635(9)	Co1–I1	2.8222(7)	Co1–N6	2.015(3)	Co1–N6	2.064(3)	2.002(2)	Co1–N6	2.044(3)
						Co1–N7	—	2.032(2)		
τ_6	0.46		0.48		0.47		0.47	0.49		0.49

indeed attractive.[44] This is also supported by electron localization function plot (Fig. S16†) which shows orientation of the nitrogen lone electron pair towards the metal ion.[45] QT-AIM analysis revealed a presence of the bond critical point (BCP) of type (3,−1) between Co1–N3 (Fig. S15†) in which the real space function values were analysed. Coordination bonds usually exhibit positive values of Laplacian of electron density ($\nabla^2 \rho(r)$) and negative values of energy density ($H(r)$) whereas both should be positive in the case of non-covalent interaction.[46] For Co1–N3 interaction, the values are 0.061 and −0.0013, respectively. Additionally, ratio $|V(r)|/G(r)$, where $V(r)$ represents potential energy density and $G(r)$ represents Lagrangian kinetic energy, should be higher than 1 for bonds possessing a degree of covalency.[47] For the studied BCP, ratio $|V(r)|/G(r)$ equals 1.076 and thus can be concluded that the bond is coordination covalent, albeit weaker, based on the aforementioned descriptors.

All complexes showed very distorted geometry of the coordination sphere between octahedral and trigonal prismatic ones as was confirmed by a continuous shape measures (deviation between the real and ideal polyhedron geometry) calculated by using the program Shape 2.1 (Table S2†).[48,49] For complexes **1–4** the coordination sphere has distorted octahedral geometry, and for complex **5** it has distorted trigonal prism shape. In all cases the deviations from ideal geometry are large (∼7) and the differences in Shape parameters for the octahedral and trigonal prismatic geometry are quite small (∼0.2–0.5 for complexes **3–5**, ∼2 for complexes **1** and **2**, Table S2†). Thus, the coordination sphere of these complexes is strongly distorted and lies in between these two geometries. The distortion of the polyhedron decreases in order **1 → 4a → 3 → 4b → 5 → 2**.

The coordination geometry was also investigated by using the newly proposed structural parameter τ_6, which is defined as follows (angles α, β and γ are the three greatest valence angles of the coordination center):[50]

$$\tau_6 = \frac{540 - (\alpha + \beta + \gamma)}{150} \quad (1)$$

This geometry index ranging from 0 (ideal octahedron) to 1 (ideal trigonal prismatic shape) is analogous to previously published τ_5 and τ_4 indices for five- and four-coordinate complexes, respectively. The τ_6 value for studied complexes **1–5** is very close to 0.5 (Table 2), which is in agreement with the

parameter obtained with Shape and confirms an actual shape of the coordination polyhedron between octahedral and prismatic trigonal.

The macrocyclic ligand is significantly bent. To express the degree of the bending, two planes have been interleaved through the system – the first one through the central atom, the pyridine nitrogen atom N1 and the two nitrogen atoms bearing the pendant arms N2 and N3, and the second plane through the central atom and the two macrocyclic oxygen atoms O1 and O2 (blue and red, respectively in Fig. 4). The angle between these two planes ranges from 75.7° (**4a**) to 77.8° (**1**).

These molecular structures of Co(II) complexes differ significantly from those obtained with **py₂-15-pyN₃O₂**, in which all seven donor atoms of the macrocycle were coordinated to the central metal atom leading to a pentagonal bipyramidal coordination sphere. This structural difference most probably arises from (i) the higher flexibility of the macrocyclic scaffold of **L**, induced by longer propylene bridges between O and NH groups and (ii) formation of less stable six-membered chelate rings for **L** in comparison with more stable five-membered chelate rings in case of **py₂-15-pyN₃O₂**. This is a typical example of the fact that the size of the macrocyclic cavity plays a crucial role in the coordination number and the geometry of the coordination sphere as well.

In the crystal packing, complexes **1** and **2** formed supramolecular 1D chains through hydrogen bonds between the two oxygen atoms of the aliphatic part of the molecule and the main pyridine ring –O···H–C$_{arom}$ (Fig. 5, S17 and S18†). These systems are further strengthened via π–π stacking interactions (C$_g$···C$_g$ distance is 4.203 Å for **1**, Fig. 5 and 4.302 Å for **2**) between the
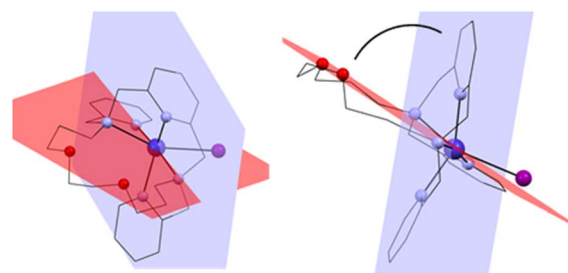

Fig. 4 Two planes interleaved through the complex cation showing the bending of the macrocyclic ligand. Front view (left) and side view (right).
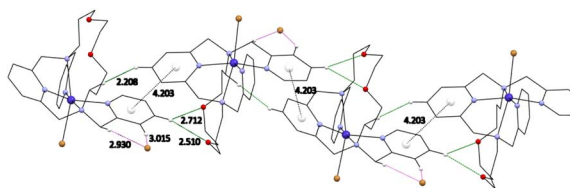
Fig. 5 Visualization of π–π stacking interactions with a centroids (white balls) distance between two pyridine rings and hydrogen bonds discussed in the text for complex **1**.

individual pyridine nuclei. The individual molecules are then linked *via* a system of additional hydrogen bonds involving the bromide anions. The main pyridine ring is thus linked to the pendant arms *via* uncoordinated bromide anions C_{arom}–H···Br···H–C_{arom}. In case of complex **2** the uncoordinated anion is half perchlorate and half iodide (Fig. S19†).

1D chains were also found in the structure of complexes **3**, **4a/b** and **5** along the *b*-axis (C_g···C_g distance is 4.209 Å, 4.258/4.026 Å and 4.211 Å, respectively, see Fig. S20 and S23†). The molecules of complex **3** are oriented in antiparallel directions and they are stabilized by hydrogen bonds *via* the isocyanate anions with aliphatic –CH_2– bonds bearing pyridine rings (Fig. S21†). In the case of complexes **3** and **5**, an uncoordinated perchlorate anion is present in the structure, which further extends the chains into a 3D network through the formation of C_{arom}–H···O–Cl–O···H–C_{arom} hydrogen bonds (Fig. S22†). The thiocyanate anion in the structure of complex **4a** occupies a site in the center of symmetry at two positions in the crystallographically independent unit. In addition, π–π stacking interaction between the pyridine nuclei of the pendant arms (C_g···C_g distance is 3.632 Å) was observed in the complex **4a** (Fig. S20†). A different situation is observed for complex **4b**, in which one of the methylpyridine pendant arms is uncoordinated and oriented in opposite direction. A 1D stacking is formed due to above-mention π–π stacking interaction however it involves the uncoordinated pendant arm and a macrocyclic pyridine ring (see Fig. S23†).

Magnetic studies

The magnetic susceptibility χ_M (defined as M/H per mole of complex with M the magnetization and H the magnetic field) between 2 and 300 K, and the field dependence of the magnetization were studied for all the complexes. The respective plots are given in Fig. 6 for **4b** and Fig. S24–S27† for the other complexes. The possibility of slow relaxation of the magnetization was tested by AC susceptibility.

The temperature dependences of the $\chi_M T$ product are very similar in this series of compounds. The main features will be described taking **4b** as an example (Fig. 6a) and some characteristic values are summarized in Table 3. For **4b**, the value of $\chi_M T$ at 300 K was 2.33 cm³ K mol⁻¹, in agreement with the calculated value of 2.48 cm³ K mol⁻¹ for a Co(II) center with spin 3/2 and g = 2.3. Upon cooling, the $\chi_M T$ product decreased slowly until 30 K before a more rapid diminution to a minimum value of 1.71 cm³ K mol⁻¹ at 2 K. This behavior is typical of Co(II) systems with second-order spin–orbit coupling (*i.e.* magnetic
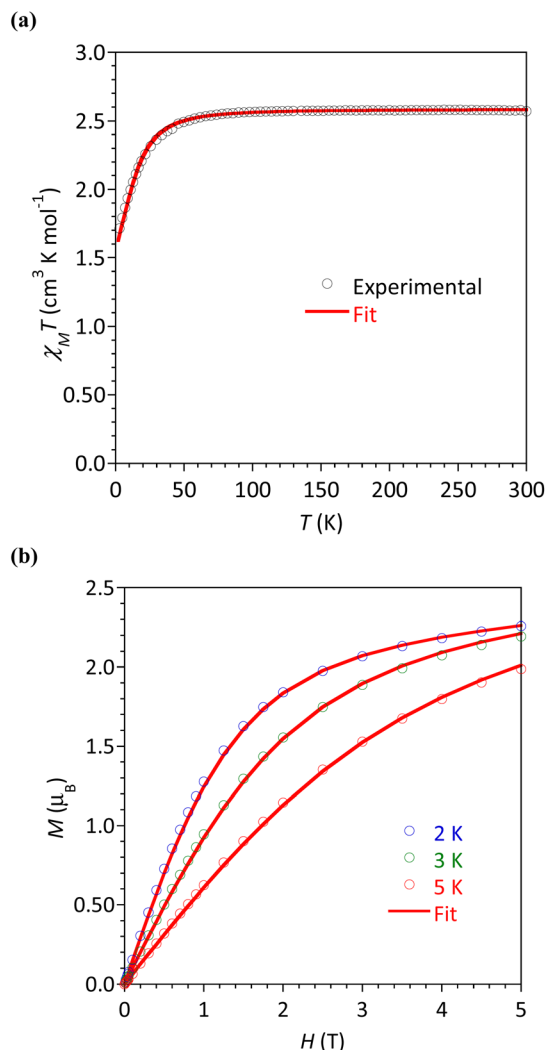

Fig. 6 Complex **4b**: (a) Temperature dependence of $\chi_M T$ and (b) field dependence of magnetization at 2, 3 and 5 K under magnetic fields up to 5 T. The lines materialize the calculated behaviors (see text).

anisotropy), and, possibly intermolecular interactions that are also expected to operate at low temperatures.

The field dependences of the magnetization were measured at temperatures ranging between 2 and 5 K (Fig. 6b and S24–S27†). The observed values at 2 K and 5 T (highest field) are between 2.14 and 2.26 μ_B, significantly lower than the expected value of 3 μ_B for a spin-only contribution for an S = 3/2 system. This is the consequence of the magnetic anisotropy resulting from ZFS for Co(II). To quantify this anisotropy the $\chi_M T$ *vs. T* and *M vs. H* curves were simultaneously analyzed using the program PHI.[27] For all complexes, positive D values were obtained but it must be stressed that the E/D ratio is large and close to 1/3. Attempts made to fit with negative values for D gave even worse E/D ratio (except for **2**). This is in agreement with geometries closer to octahedral (*vide supra*) known to promote $D > 0$.[9] For complex **5** we could not obtain a satisfactory modeling, even taking into account intermolecular interactions (zj'), suggested by the marked drop of $\chi_M T$ at 2 K. The absolute D and E values are in good agreement with those obtained by theoretical

Table 3 Selected experimental and calculated magnetic parameters for complexes 1–5

Compound	χT (300 K)	M (μ_B) (2 K)	D (cm^{-1})	E (cm^{-1})	E/D	g
1·MeOH	2.42	2.15	16.17 ± 0.4	4.9 ± 0.2	0.30	2.272 ± 0.001
Calculated[a]			−17.38	−5.44	0.31	2.265
2·MeOH	2.59	2.15	−17.4 ± 0.4	5.3 ± 0.4	0.30	2.354 ± 0.002
Calculated[a]			−23.61	−6.35	0.27	2.278
3·MeOH	2.58	2.26	12.8 ± 0.3	2.8 ± 0.3	0.22	2.231 ± 0.001
Calculated[a]			−14.96	−4.73	0.31	2.256
4a·0.25 MeOH	—	—	—	—	—	—
Calculated[a]			−19.29	−5.37	0.28	2.264
4b	2.33	2.14	17.0 ± 0.3	3.4 ± 0.2	0.20	2.348 ± 0.001
Calculated[a]			−17.40	−5.63	0.32	2.264
5·MeOH	2.47	2.23	[b]	[b]	[b]	[b]
Calculated[a]			−15.34	−4.18	0.27	2.250

[a] By CASSCF/NEVPT2. [b] No satisfactory fit could be obtained for **5**.

calculations (*vide infra*), the difference of sign is not relevant for system with large rhombicity (*E/D* ratio close to the maximal value 1/3).[51]

In order to confirm obtained experimental *D* and *E* values, the post-Hartree–Fock CASSCF(7,5)/NEVPT2 calculations were performed. Results are given in Table 3. The *D* values for all the complexes are negative and found between −24 and −15 cm^{-1}. The calculated individual non-zero contributions to *D*-tensor for complexes **1–5** are given in Table S3† and it is clear that the contribution of the first excited state has always the largest negative value, thus represents the main contribution to *D*-tensor and therefore the overall *D*-values are negative in sign.

The absolute *D*-values are in good agreement with the experimental ones including also large values of rhombic parameter *E* or *E/D* ratio close to the maximal value 1/3. On the other hand, they differ in sign which is not relevant for systems with a large rhombicity. In such a case the system has uniaxial magnetic anisotropy regardless the sign of *D*-value.[51] It is worth noting that norms of projected states of the effective

Hamiltonian are near 1, suggesting that the results obtained from calculations should be reliable as there are no low-lying 2nd excited states.

The energy diagrams of the d-orbital splitting, ligand-field terms and ligand-field multiplets are shown in Fig. 7. The splitting of d-orbitals is far from that of an ideal octahedral or trigonal prismatic ligand field, which is in accordance with strongly distorted coordination geometry in between octahedral and trigonal prismatic.

The d-orbital splitting resembles the splitting obtained for previously studied trigonal prismatic Co(II) complexes with **17-pyN$_5$-pip**,[25] especially those with NCO$^-$, NCS$^-$ and NCSe$^-$ coligands. Moreover, calculated *D*-values were in a similar range (*ca.* 30–50% larger, *i.e.* −31 to −35 cm^{-1}) in comparison with studied complexes **1–5**.

AC susceptibility responses have been investigated for each complex but a maximum for χ''_M above 2 K was only detected for complex **4b** when applying a dc field. The field dependence of the AC signal at 2 K indicated an optimal field of 3 kOe
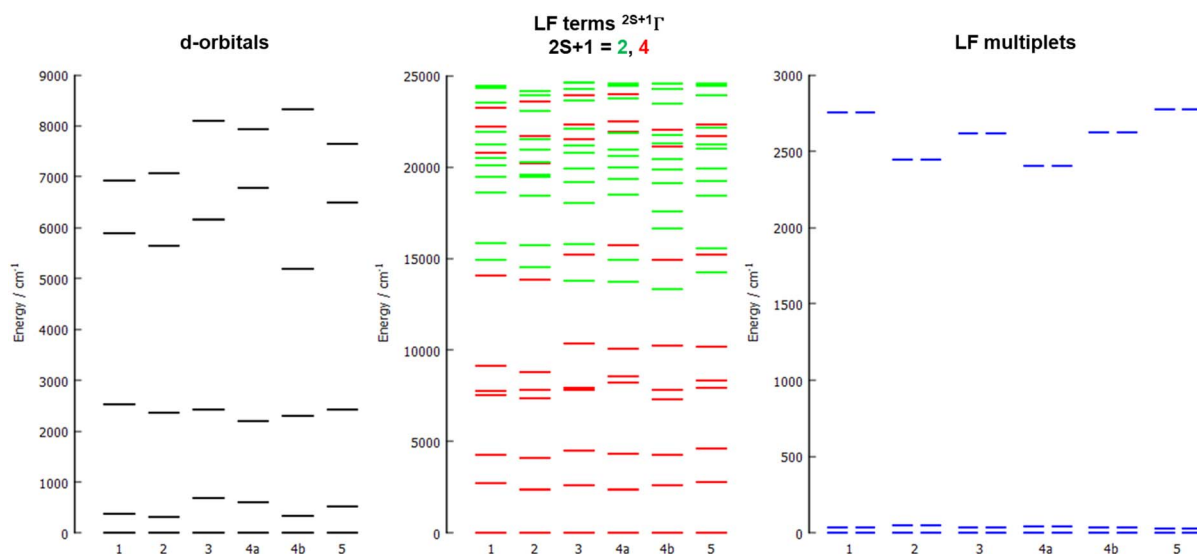

Fig. 7 The d-orbital splitting calculated by *ab initio* ligand field theory (AILFT) (left), low-lying ligand-field terms with various multiplicities (middle), and ligand-field multiplets (right), all obtained from CASSCF/NEVPT2 calculations for all studied complexes **1–5**.

(Fig. S28†). Subsequently, the AC signals for **4b** in $H_{DC} = 3$ kOe were measured scanning frequencies from 1 to 1500 Hz every 0.2 K between 2 and 7 K (Fig. 8a and S29†). The relaxation time, τ, was obtained by analyzing the χ''_M versus ν data for each temperature with the generalized Debye model,[52] results are plotted as $1/\tau$ (log scale) versus T in Fig. 8b. This behavior was well reproduced until 2.6 K considering Raman and direct relaxation mechanisms (eqn (2)), best fit gave $C = 0.02 \pm 0.01$ K^{-n} s^{-1}, $n = 9.3 \pm 0.4$ and $B = 14\,000 \pm 3000$ K^{-1} T^{-4} s^{-1}. Attempts considering Raman and QTM processes gave poor quality fits, and an Orbach mechanism is excluded for a system with positive D.[53]

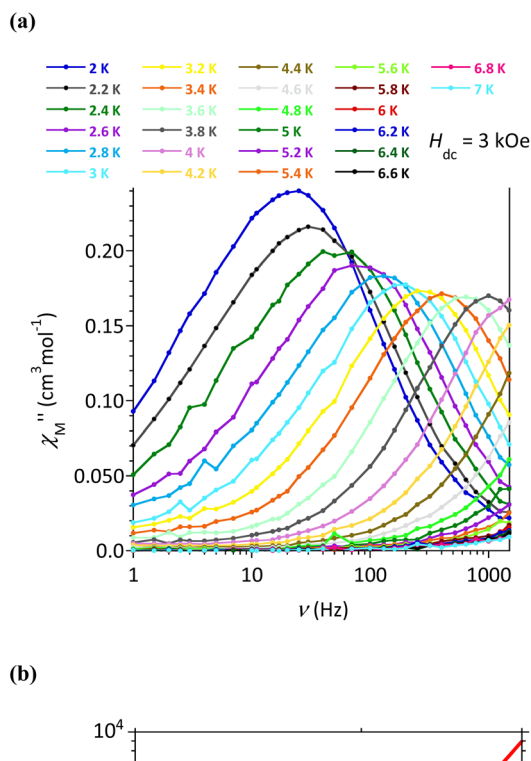$$\tau^{-1} = CT^n + BH^4T \qquad (2)$$

(a)

(b)

Fig. 8 Compound **4b**: (a) Frequency dependence of the out-of-phase component of the ac susceptibility with $H_{DC} = 3$ kOe and (b) temperature dependence of the relaxation time. The line materializes the best fit (see text).

Conclusion

A new macrocyclic ligand containing two 2-methylpyridine pendant arms was prepared and involved in the preparation of a series of Co(II) complex with one monovalent coligand (X = Br^-, I^-, NCO^-, NCS^- and N_3^-). All complexes are six-coordinate with a strongly distorted coordination sphere lying in between octahedral and trigonal prismatic geometry. Although the macrocyclic ligand is potentially heptadentate, only its nitrogen atoms are involved in the coordination to Co(II), the two oxygen donor atoms are not due to a large flexibility of the 17-membered macrocycle. These complexes show modest magnetic anisotropy with positive D-values but with E/D ratio close to 1/3, regardless the different coligand. Interestingly, complex **4b** was found to behave as a field-induced SMM with magnetization relaxation driven by a direct and Raman mechanisms.

Data availability

The data supporting this article have been included as part of the ESI.† Crystallographic data for **1**, **2**, **3**, **4a**, **4b** and **5** has been deposited at the CCDC database under deposition numbers 2344172, 2344178, 2344177, 2344175, 2371458, and 2344176.

Conflicts of interest

There are no conflicts to declare.

Acknowledgements

References

1 R. Sessoli, D. Gatteschi, A. Caneschi and M. A. Novak, *Nature*, 1993, **365**, 141.
2 D. Gatteschi, R. Sessoli and J. Villain, *Molecular Nanomagnets*, Oxford University Press, Oxford, U.K., 2006.
3 M. Mannini, F. Pineider, P. Sainctavit, C. Danieli, E. Otero, C. Sciancalepore, A. M. Talarico, M.-A. Arrio, A. Cornia and D. Gatteschi, *Nat. Mater.*, 2009, **8**, 194.
4 R. E. Winpenny, *Angew. Chem., Int. Ed.*, 2008, **47**, 7992.
5 L. Bogani and W. Wernsdorfer, *Nat. Mater.*, 2008, **7**, 179.
6 A. M. Ako, I. J. Hewitt, V. Mereacre, R. Clérac, W. Wernsdorfer, C. E. Anson and A. K. Powell, *Angew. Chem.*, 2006, **118**, 229.
7 F. Neese and D. A. Pantazis, *Faraday Discuss.*, 2011, **148**, 229.
8 A. Zabala-Lekuona, J. M. Seco and E. Colacio, *Coord. Chem. Rev.*, 2021, **441**, 213984.
9 V. Vieru, S. Gómez-Coca, E. Ruiz and L. F. Chibotaru, *Angew. Chem., Int. Ed.*, 2024, **63**, e202303146.

10 P. Antal, B. Drahoš, R. Herchel and Z. Trávníček, *Inorg. Chem.*, 2016, **55**(12), 5957.

11 B. Drahoš, R. Herchel and Z. Trávníček, *Inorg. Chem.*, 2015, **54**(7), 3352.

12 J.-P. Sutter, V. Béreau, V. Jubault, K. Bretosh, C. Pichon and C. Duhayon, *Chem. Soc. Rev.*, 2022, **51**, 3280–3313.

13 P. Kumar Sahu, R. Kharel, S. Shome, S. Goswami and S. Konar, *Coord. Chem. Rev.*, 2023, **475**, 214871.

14 T. G. Ashebr, H. Li, X. Ying, X.-L. Li, C. Zhao, S. Liu and J. Tang, *ACS Mater. Lett.*, 2022, **4**, 307–319.

15 J. Li, Y. Yang, Q. Yu, G. Su and W. Liu, *J. Phys. Chem. C*, 2024, **128**, 4882–4890.

16 J. Juráková and I. Šalitroš, *Monatsh. Chem.*, 2022, **153**, 1001–1036.

17 A. Sarkar, S. Dey and G. Rajaraman, *Chem.–Eur. J.*, 2020, **26**, 14036–14058.

18 S. Ghosh, S. Kamilya, M. Das, S. Mehta, M.-E. Boulon, I. Nemec, M. Rouzières, R. Herchel and A. Mondal, *Inorg. Chem.*, 2020, **59**, 7067–7081.

19 A. K. Bar, C. Pichon and J.-P. Sutter, *Coord. Chem. Rev.*, 2016, **308**, 346–380.

20 U. Luening, *Liebigs Ann. Chem.*, 1987, **11**, 949–955.

21 B. Drahoš, J. Kotek, P. Hermann, I. Lukeš and É. Tóth, *Inorg. Chem.*, 2010, **49**, 3224–3238.

22 B. Drahoš, R. Herchel and Z. Trávníček, *Inorg. Chem.*, 2017, **56**, 5076–5088.

23 P. Antal, B. Drahoš, R. Herchel and Z. Trávníček, *Eur. J. Inorg. Chem.*, 2018, **2018**, 4286–4297.

24 B. Drahoš, I. Císařová, O. Laguta, V. T. Santana, P. Neugebauer and R. Herchel, *Dalton Trans.*, 2020, **49**, 4425–4440.

25 E. Zahradníková, J.-P. Sutter, P. Halaš and B. Drahoš, *Dalton Trans.*, 2023, **52**, 18513–18524.

26 O. Kahn, *Molecular Magnetism*, VCH, Weinheim, 1993.

27 N. F. Chilton, R. P. Anderson, L. D. Turner, A. Soncini and K. S. Murray, *J. Comput. Chem.*, 2013, **34**, 1164–1175.

28 G. M. Sheldrick, *Acta Crystallogr., Sect. C: Struct. Chem.*, 2015, **71**, 3–8.

29 P. W. Betteridge, J. R. Carruthers, R. I. Cooper, K. Prout and D. J. Watkin, *J. Appl. Crystallogr.*, 2003, **36**, 1487.

30 O. V. Dolomanov, L. J. Bourhis, R. J. Gildea, J. A. K. Howard and H. Puschmann, *J. Appl. Crystallogr.*, 2009, **42**, 339–341.

31 C. F. Macrae, I. J. Bruno, J. A. Chisholm, P. R. Edgington, P. McCabe, E. Pidcock, L. Rodriguez-Monge, R. Taylor, J. van de Streek and P. A. Wood, *J. Appl. Crystallogr.*, 2008, **41**, 466–470.

32 E. Zahradníková, R. Herchel, I. Šalitroš, I. Císařová and B. Drahoš, *Dalton Trans.*, 2020, **49**, 9057–9069.

33 (*a*) F. Neese, F. Wennmohs, U. Becker and C. Riplinger, *J. Chem. Phys.*, 2020, **152**(22), 224108; (*b*) F. Neese, *Wiley Interdiscip. Rev.: Comput. Mol. Sci.*, 2022, e1606.

34 A. D. Becke, *Phys. Rev. A*, 1988, **38**, 3098.

35 F. Weigend and R. Ahlrichs, *Phys. Chem. Chem. Phys.*, 2005, **7**(18), 3297.

36 F. Neese, *J. Comput. Chem.*, 2003, **24**(14), 1740.

37 F. Weigend, *Phys. Chem. Chem. Phys.*, 2006, **8**(9), 1057.

38 J. D. Rolfes, F. Neese and D. A. Pantazis, *J. Comput. Chem.*, 2020, **41**(20), 1842.

39 F. Neese, F. Wennmohs, A. Hansen and U. Becker, *Chem. Phys.*, 2009, **356**(1–3), 98.

40 A. Hellweg, C. Hättig, S. Höfener and W. Klopper, *Theor. Chem. Acc.*, 2007, **117**(4), 587.

41 R. F. Bader, *Acc. Chem. Res.*, 1985, **18**(1), 9–15.

42 T. Lu and F. Chen, *J. Comput. Chem.*, 2012, **33**(5), 580–592.

43 L. Havlíček, R. Herchel, I. Nemec and P. Neugebauer, *Polyhedron*, 2022, **223**, 115962.

44 E. R. Johnson, S. Keinan, P. Mori-Sánchez, J. Contreras-García, A. J. Cohen and W. Yang, *J. Am. Chem. Soc.*, 2010, **132**(18), 6498–6506.

45 A. D. Becke and K. E. Edgecombe, *J. Chem. Phys.*, 1990, **92**(9), 5397–5403.

46 I. V. Ananyev, N. A. Bokach and V. Y. Kukushkin, *Acta Crystallogr., Sect. B: Struct. Sci., Cryst. Eng. Mater.*, 2020, **76**(3), 436–449.

47 E. Espinosa, I. Alkorta, J. Elguero and E. Molins, *J. Chem. Phys.*, 2002, **117**(12), 5529–5542.

48 D. Casanova, P. Alemany, J. M. Bofill and S. Alvarez, *Chem.–Eur. J.*, 2003, **9**(6), 1281–1295.

49 S. Alvarez, *Dalton Trans.*, 2005, (13), 2209–2233.

50 J. Moncol, *Czech Chem. Soc. Symp. Ser.*, 2023, **21**, 147.

51 I. Nemec, R. Herchel, M. Kern, P. Neugebauer, J. van Slageren and Z. Travnicek, *Materials*, 2017, **10**, 249.

52 C. Dekker, A. F. M. Arts, H. W. de Wijn, A. J. van Duyneveldt and J. A. Mydosh, *Phys. Rev. B: Condens. Matter Mater. Phys.*, 1989, **40**, 11243.

53 S. Gómez-Coca, A. Urtizberea, E. Cremades, P. J. Alonso, A. Camón, E. Ruiz and F. Luis, *Nat. Commun.*, 2014, **5**, 5300.